ACS APPLIED MATERIALS & INTERFACES

www.acsami.org

Research Article

Excellent UV Resistance of Polylactide by Interfacial Stereocomplexation with Double-Shell-Structured TiO_2 Nanohybrids

Ying Cao, Pengwu Xu, Pei Lv, Pieter Jan Lemstra, Xiaoxia Cai, Weijun Yang, Weifu Dong, Mingqing Chen, Tianxi Liu, Mingliang Du, and Piming Ma*

Cite This: *ACS Appl. Mater. Interfaces* 2020, 12, 49090–49100

Read Online

ACCESS | Metrics & More | Article Recommendations | Supporting Information

ABSTRACT: The durable application of polylactide (PLA) under atmospheric conditions is restricted by its poor ultraviolet (UV) stability. To improve the UV stability of polymers, titanium dioxide (TiO_2) is often used as a UV light capture agent. However, TiO_2 is also a photocatalytic agent, with detrimental effects on the polymer properties. To overcome these two conflicting issues, we used the following approach. TiO_2 nanoparticles were first coated with silicon dioxide (SiO_2) (with a SiO_2 shell content of 5.3 wt %). Subsequently, poly(D-lactide) (PDLA) was grafted onto TiO_2@SiO_2 nanoparticles, approximately 20 wt %, via a ring-opening polymerization of D-lactide to obtain well-designed double-shell TiO_2@SiO_2-*g*-PDLA nanohybrids. These double-shell nanoparticles could be well dispersed in a poly(L-lactide) (PLLA) matrix making use of the stereocomplexation between the two enantiomers. In our concept, the inner SiO_2 shell on the TiO_2 nanoparticles prevents the direct contact between TiO_2 and the PLLA matrix and hence considerably restricts the detrimental photocatalytic effect of TiO_2 on PLLA degradation. Additionally, the outer PDLA shell facilitates an improved dispersion of these nanohybrid particles by interfacial stereocomplexation with its enantiomer PLLA. As a consequence, the PLLA/TiO_2@SiO_2-*g*-PDLA nanocomposites simultaneously possess excellent UV-shielding property, high(er) tensile strength (>60 MPa), and superior UV resistance, for example, the mechanical properties remain at a level of >90% after 72 h of UV irradiation. In our view, this work provides a novel strategy to make advanced PLA nanocomposites with improved mechanical properties and excellent UV resistance, which enables potential application of PLA in more critical areas such as in durable packaging and fiber/textile applications.

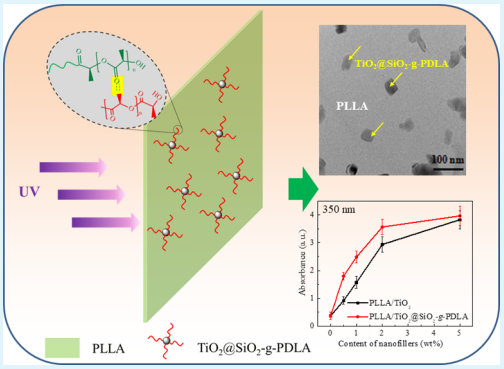

KEYWORDS: *PLA, TiO_2, interfacial stereocomplexation, double-shell structure, UV resistance*

1. INTRODUCTION

In recent years, the development of bio-based and biocompostable materials has drawn increasing attention because of the environmental and sustainability concerns. Polylactide (PLA) materials including poly(L-lactide) (PLLA) and poly(D-lactide) (PDLA) have become popular in the area of green packaging and medical devices because of its compostability and biocompatibility. Besides, many other advantages of PLA, that is, its high strength, being bio-based, and ease of processability, made it a potential candidate for replacing traditional petroleum-based plastics.[1−6] In the meantime, some shortcomings such as high brittleness, poor heat and ultraviolet (UV) stability, and lack of functionality also limited the application range of PLA materials. Lots of studies have been carried out, resulting in PLA materials with good toughness or functionalities such as conductivity, antibacterial activity, and self-healing.[7−11] However, the aging and degradation issues of PLA under UV irradiation have not been investigated yet in great detail. The photolysis of PLA follows the Norrish type II decomposition mechanism with main chain scission to form short(er) molecules, leading to the deterioration in mechanical properties.[12−14] Such deterioration would strongly influence the safety and service life of the corresponding products and thus limit the practical applications of PLA materials. Therefore, fabricating UV-resistant PLA materials has been of interest in both academia and industry.

Nano-sized titanium dioxide (TiO_2) has inherent photocatalytic activity and UV-shielding properties.[15−23] Numerous studies have been performed on blending PLA with TiO_2 nanoparticles to prepare UV-shielding nanocomposites.[24−29] Zhuang et al.[30] designed PLA/TiO_2 nanocomposites by in situ polymerization and achieved high strength and UV-shielding property. However, the degradation rate of PLA increased with the TiO_2 content because the photocatalytic activity of TiO_2 could result in decomposition of the PLA matrix. Free radicals

Received: August 10, 2020
Accepted: October 7, 2020
Published: October 19, 2020

https://dx.doi.org/10.1021/acsami.0c14423
ACS Appl. Mater. Interfaces 2020, 12, 49090−49100

Scheme 1. Preparation of (1) TiO_2@SiO_2 Nanoparticles, (2) TiO_2@SiO_2-*g*-PDLA Nanohybrids, and (3) PLA/TiO_2@SiO_2-*g*-PDLA Nanocomposites

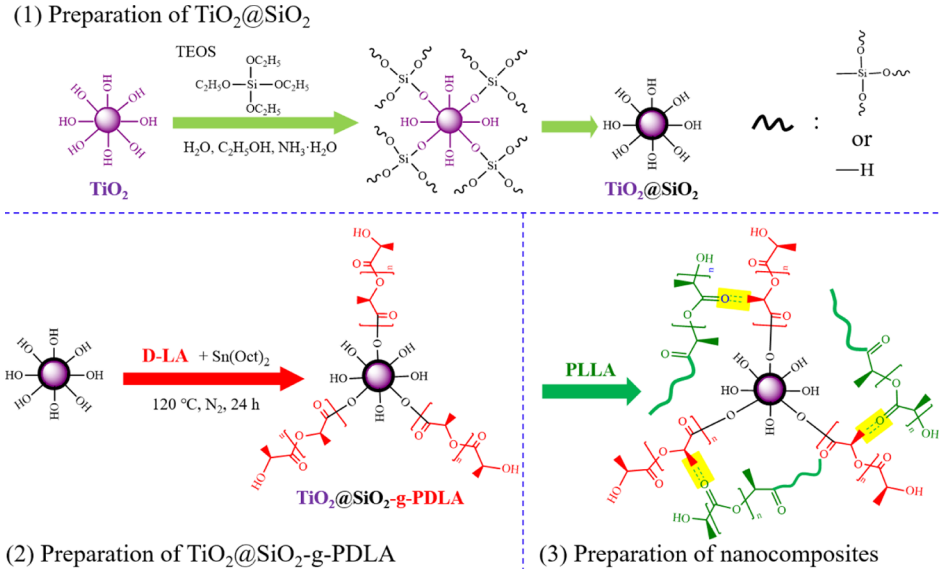

with high reactivity could be generated by TiO_2 after absorbing UV light, which will attack the neighboring polymer chains in the PLA matrix, and consequently, lead to decomposition.[31,32] In addition, the poor compatibility between inorganic nanoparticles and the matrix is always one of the major issues for high-performance PLA nanocomposites. The agglomeration of nanoparticles usually results in poor mechanical properties, for example, low(er) strength and toughness. Thus, extra modification is required to avoid aggregation and achieve a fine dispersion of nanoparticles. Nakayama et al.[33] prepared PLA/TiO_2 nanocomposites via solution-casting, and an improved dispersion of TiO_2 was achieved after the modification of TiO_2 with a carboxylic acid and a long-chain alkyl amine. However, limited interfacial adhesion was created due to lack of interfacial bonding and consequently poor mechanical properties. It was found that interfacial stereocomplexation was proved to be an effective way to in situ create a strong affinity between two different components accompanied by much better dispersion of nanofillers.[6−10]

To summarize, it is still challenging to make robust PLA nanocomposites in combination with both excellent mechanical and UV-resistant performances. To achieve this target, specifically in the PLA/TiO_2 nanocomposites, the poor affinity and the nondesirable photocatalytic effect of TiO_2 have to be solved.

In this work, we addressed an effective route to make UV-stable PLLA/TiO_2@SiO_2-*g*-PDLA nanocomposites. The photocatalytic effect of TiO_2 was restricted within the particles by designing a double-shell-structured TiO_2@SiO_2-*g*-PDLA nanohybrids, where the SiO_2 inner shell could effectively prevent the free radicals from attacking the PLLA matrix. Meanwhile, the outer PDLA shell increases the interfacial adhesion between the nanohybrids and the PLLA matrix via strong physical bonding, that is, the so-called stereocomplexation. Therefore, this work provides a new strategy to make robust PLA nanocomposites with superior UV resistance, which may expand its application range in more advanced packaging and fiber/textile fields.

2. EXPERIMENTAL SECTION

2.1. Materials. Poly (L-lactide) (PLLA, M_n = 180 kDa, PDI = 1.42) was purchased from Zhejiang Hisun Biomaterials Co., Ltd. D-Lactide (99% purity) was provided by Nantong Jiuding Biological Engineering Co., Ltd. Nano TiO_2 (>99.8%, ~40 nm) was purchased from Shanghai Macklin Biochemical Co., Ltd. Sodium hexametaphosphate [$(NaPO_3)_6$, CP], tetraethyl orthosilicate (TEOS, AR), ethanol (AR), toluene ($C_6H_5CH_3$, AR), methanol (CH_3OH, AR), ammonia ($NH_3{\cdot}H_2O$, AR), and chloroform ($CHCl_3$, AR) were provided by Sinopharm Group Chemical Reagent Co., Ltd. Stannous caprylate ($Sn(Oct)_2$, AR) from Shanghai Aladdin Reagent Co., Ltd. was used as the catalyst for the ring-opening polymerization of D-lactide.

2.2. Experiments. *2.2.1. Preparation of TiO_2@SiO_2 Nanoparticles.* TiO_2@SiO_2 nanoparticles were obtained by the hydrolysis of TEOS on the surface of TiO_2. The specific synthesis process was as follows. NanoTiO_2 (1 g), deionized water (150 mL), and $(NaPO_3)_6$ (50 mg) were transferred into a beaker and dispersed ultrasonically for 30 min. Then, ethanol with 25 mL of $NH_3{\cdot}H_2O$ and 25 mL of TEOS were added separately to the beaker under stirring. After the addition, the mixture was kept for 5 h at room temperature. Finally, TiO_2@SiO_2 nanoparticles were obtained after purification with deionized water.

2.2.2. Preparation of TiO_2@SiO_2-g-PDLA Nanohybrids. PDLA was grafted onto the surface of TiO_2@SiO_2 nanoparticles by ring-opening polymerization of D-lactide forming TiO_2@SiO_2-*g*-PDLA nanohybrids. The procedure is as follows: D-lactide (20 g), TiO_2@SiO_2 (1 g), and $Sn(Oct)_2$ (0.6 g) were brought into contact with each other to react in a three-necked flask (nitrogen) at 120 °C for 24 h. The nanohybrids were recovered by precipitation in cold methanol and then washed and centrifuged with chloroform to remove the remaining D-lactide and free PDLA. TiO_2@SiO_2-*g*-PDLA nanohybrids were then dried in a vacuum oven at 60 °C.

2.2.3. Preparation of PLLA/TiO_2@SiO_2-g-PDLA Nanocomposites. PLLA/TiO_2@SiO_2-*g*-PDLA nanocomposites and the corresponding films were prepared via a solution-casting method using chloroform as a solvent. The content of TiO_2@SiO_2-*g*-PDLA nanohybrids was designed as 0.5−5 wt %. For comparison, PLLA and PLLA/TiO_2 nanocomposites were prepared in the same way as reference. The preparation routes of TiO_2@SiO_2, TiO_2@SiO_2-*g*-PDLA nanohybrids, and the PLA nanocomposites are illustrated in Scheme 1.

2.3. Characterization. *2.3.1. Fourier-Transform Infrared Spectroscopy.* An FT-IR spectrometer (Nicolet 6700, USA) was used to analyze the TiO_2, TiO_2@SiO_2, and TiO_2@SiO_2-*g*-PDLA nanohybrids

https://dx.doi.org/10.1021/acsami.0c14423
ACS Appl. Mater. Interfaces 2020, 12, 49090−49100

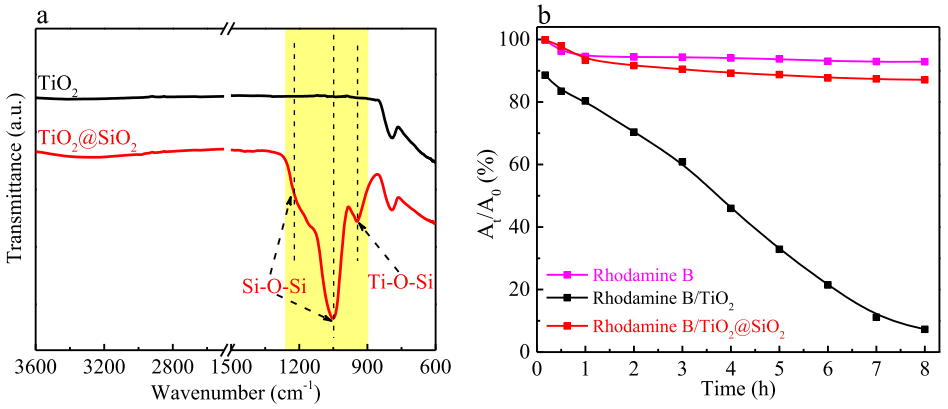

Figure 1. (a) FTIR spectra and (b) photocatalytic activities of TiO_2 and TiO_2@SiO_2 nanoparticles.

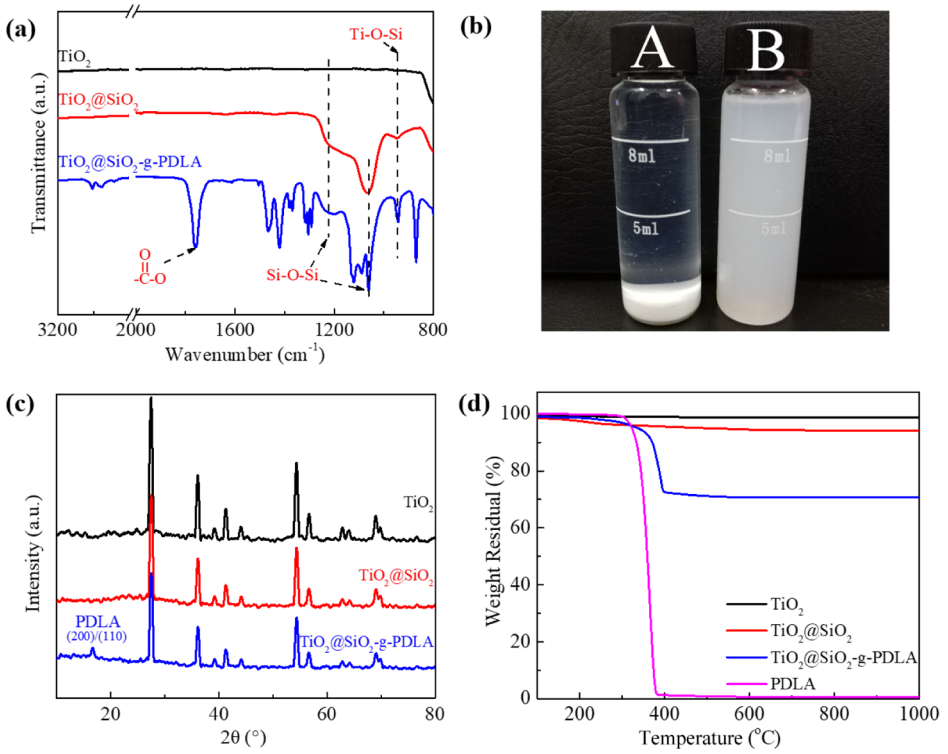

Figure 2. (a) FT-IR spectra of TiO_2, TiO_2@SiO_2, and TiO_2@SiO_2-*g*-PDLA nanohybrids, (b) images of the (A) TiO_2/PDLA physical mixture and (B) TiO_2@SiO_2-*g*-PDLA nanohybrids in chloroform for 72 h; (c) XRD patterns and (d) TGA curves of TiO_2, TiO_2@SiO_2, and TiO_2@SiO_2-*g*-PDLA nanohybrids.

in an attenuation total reflection mode. The scanning range was 400−4000 cm^{-1} with a resolution of 4 cm^{-1}.

2.3.2. Photocatalytic Activity. A Rhodamine B solution (5 mg/L) without nanoparticles and a solution containing TiO_2 (20 mg) and TiO_2@SiO_2 (20 mg) nanoparticles were irradiated with an UV lamp for 8 h (wavelength: 360 nm, power: 300 W). Every hour, 5 mL of rhodamine B was taken to obtain the supernatant by centrifugation.

2.3.3. UV−Visible Spectrophotometry. The UV absorption values of rhodamine B solution exposed to UV irradiation for different times were measured using a UV−visible spectrophotometer (UV−vis) (TU-1901, China) with a wavelength scanning range of 200−800 nm. The relative content (I) of rhodamine B after irradiation is calculated using the following formula

$$I = \frac{A_t}{A_0} \times 100\%$$

where A_0 and A_t represent the UV absorption values of rhodamine B solution irradiated by UV light for 0 and t h, respectively. The results were used to assess the photocatalytic activities of TiO_2 and TiO_2@SiO_2 nanoparticles.

2.3.4. Atomic Force Microscopy. TiO_2 and TiO_2@SiO_2-*g*-PDLA were ultrasonically dispersed in chloroform (0.5 mg/mL) separately. The resultant TiO_2 and TiO_2@SiO_2-*g*-PDLA suspensions (5 μL) were then deposited on the surface of a silicon wafer. The morphology of TiO_2 and TiO_2@SiO_2-*g*-PDLA nanohybrids was characterized by AFM (MultiMode 8 AFM system, Germany) in the peak force quantitative nanomechanical properties test (QNM) mode.

2.3.5. Thermogravimetric Analysis. The thermal decomposition behaviors of TiO_2, TiO_2@SiO_2, TiO_2@SiO_2-*g*-PDLA nanohybrids, and PDLA were studied from 30 to 600 °C (10 °C/min) in a N_2 atmosphere through thermogravimetric analysis (TGA) (1100SF, Switzerland).

2.3.6. X-ray Diffraction Spectroscopy. Before testing, TiO_2, TiO_2@SiO_2, and TiO_2@SiO_2-*g*-PDLA nanohybrids were annealed at 90 °C for 2 h, and the PLLA, PLLA/TiO_2, and PLLA/TiO_2@SiO_2-*g*-PDLA nanocomposites were heated to 200 °C to hold for 3 min and

https://dx.doi.org/10.1021/acsami.0c14423
ACS Appl. Mater. Interfaces 2020, 12, 49090−49100

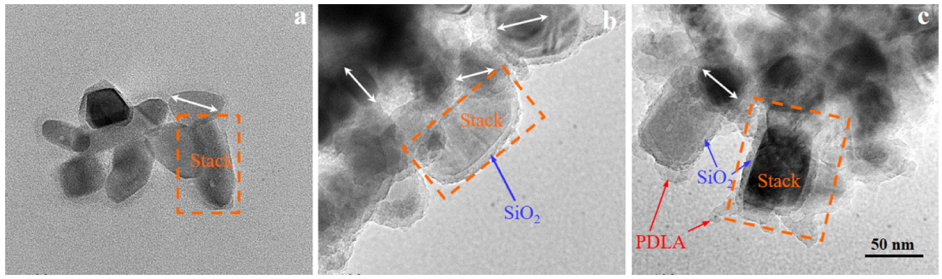

Figure 3. TEM images (on the same scale) of (a) TiO_2, (b) TiO_2@SiO_2, and (c) TiO_2@SiO_2-*g*-PDLA nanohybrid particles.

then cooled to 30 °C at a cooling rate of 10 °C/min. Then, an X-ray diffraction spectroscope (Bruker AXS D8, Germany) was used to observe the crystal structure of the samples with scan angles from 5 to 90° at a scanning speed of 3°/min.

2.3.7. Transmission Electron Microscopy. TiO_2, TiO_2@SiO_2, and TiO_2@SiO_2-*g*-PDLA nanohybrids were ultrasonically dispersed in chloroform (0.5 mg/mL) separately. Then, the suspensions (5 μL) were dropped onto a copper mesh. After volatilization of chloroform, the morphology of TiO_2, TiO_2@SiO_2, and TiO_2@SiO_2-*g*-PDLA was observed with a transmission electron microscope (200 kV, JEOL-JEM-2100, Japan).

2.3.8. Mechanical Properties. The tensile properties of PLLA nanocomposites irradiated with an UV lamp (300 W) were measured using a tensile tester (Instron 5967, USA) at room temperature according to GBT529-2008 standard at a crosshead speed of 10 mm min^{-1}. Five measurements of each sample were performed and the averaged values are presented.

3. RESULTS AND DISCUSSION

3.1. Structural Analysis of TiO_2@SiO_2-*g*-PDLA Nanohybrids. TiO_2 nanoparticles were coated with a SiO_2 shell through hydrolysis and condensation reactions of TEOS. Figure 1a shows the FT-IR spectra of TiO_2 and TiO_2@SiO_2 nanoparticles, indicating the chemical structure of nanoparticles before and after coating. Compared with the FT-IR spectrum of TiO_2, TiO_2@SiO_2 shows new visible FT-IR peaks at 1229, 1071, and 941 cm^{-1}. According to the literature, the absorption peaks at 1229 and 1071 cm^{-1} correspond to the stretching vibrations of Si−O−Si,[34] and the absorption peak at 941 cm^{-1} corresponds to the stretching vibrations of Ti−O−Si.[35] These results indicate that SiO_2 is chemically bonded to the surface of TiO_2 nanoparticles. In addition, the influence of the SiO_2 layer on the photocatalytic activity of nanoparticles was also studied, as shown in Figure 1b.

The photocatalytic activities of TiO_2 and TiO_2@SiO_2 nanoparticles were evaluated by tracing the relative content of rhodamine B in solution, as mentioned in the Experimental Section. As can be inferred from Figure 1b, the relative content of rhodamine B in rhodamine B/TiO_2 solution sharply decreases with UV irradiation time, and the value is even less than 10% after 8 h of UV irradiation. On the contrary, the rhodamine B content in the neat rhodamine B solution and in rhodamine B/TiO_2@SiO_2 solution remains as high as 90% after UV irradiation. In other words, the presence of TiO_2 nanoparticles significantly accelerated the decomposition of rhodamine B because of its inherent photocatalytic activity. In detail, the electron (e^-_{cb}) of TiO_2 nanoparticles would absorb energy from UV light and jump from the valence band to the conduction band, leaving a hole in the valence band (h^+_{vb}). Electrons in the conduction band react easily with O_2 to form $^{\bullet}O_2$, while the holes react easily with H_2O to form $^{\bullet}OH$. Then, the organic matter can be decomposed into H_2O and O_2

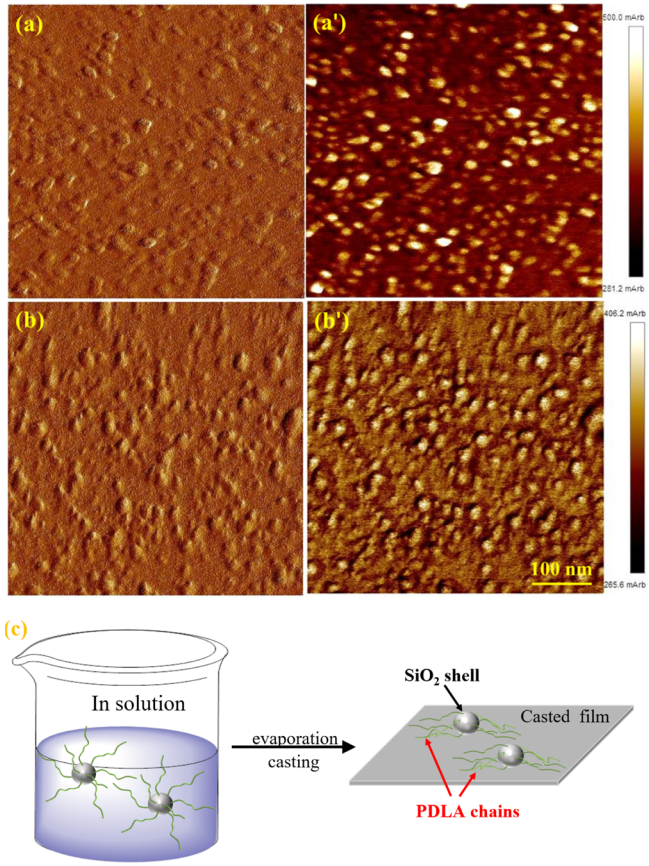

Figure 4. AFM images (on the same scale) of (a/a') TiO_2 and (b/b') TiO_2@SiO_2-*g*-PDLA nanohybrids in the (a/b) peak force error mode and (a'/b') modulus mode. (c) Schematic diagram of dispersion of TiO_2@SiO_2-*g*-PDLA nanohybrids before and after casting.

during the contact with $^{\bullet}O_2$ and $^{\bullet}OH$ with high chemical activity.[30] Obviously, TiO_2@SiO_2 nanoparticles did not exhibit obvious photocatalytic effects after coating with the SiO_2 layer, which can prevent the contact between TiO_2 and rhodamine B, that is, preventing the active $^{\bullet}O_2$ and $^{\bullet}OH$ attacking the organic matter nearby (e.g., rhodamine B). FT-IR and photocatalytic activity tests indicate that the chemically bonded SiO_2 ensures a low photocatalytic activity of the TiO_2@SiO_2 nanoparticles.

Furthermore, TiO_2@SiO_2-*g*-PDLA nanohybrids were prepared through a ring-opening polymerization of D-lactide on the surface of TiO_2@SiO_2 nanoparticles. FT-IR, XRD, and TGA analyses are used to characterize the chemical and physical structures of the TiO_2@SiO_2-*g*-PDLA nanohybrids, as shown in Figure 2.

https://dx.doi.org/10.1021/acsami.0c14423
ACS Appl. Mater. Interfaces 2020, 12, 49090−49100

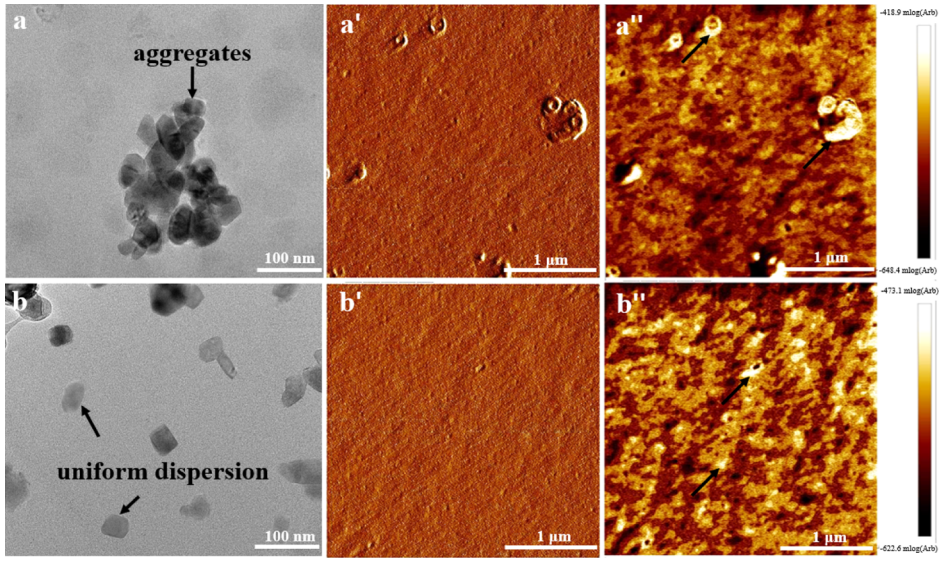

Figure 5. TEM images of (a) PLLA/TiO_2 and (b) PLLA/TiO_2@SiO_2-*g*-PDLA nanocomposites; AFM peak force error images of (a') PLLA/TiO_2 and (b') PLLA/TiO_2@SiO_2-*g*-PDLA nanocomposites; and AFM modulus images of (a'') PLLA/TiO_2 and (b'') PLLA/TiO_2@SiO_2-*g*-PDLA nanocomposites. The content of nanofillers is 2 wt % in all nanocomposites.

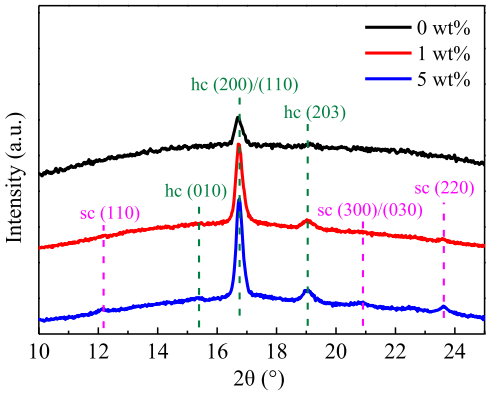

Figure 6. WAXD patterns of PLLA/TiO_2@SiO_2-*g*-PDLA nanocomposites with different TiO_2@SiO_2-*g*-PDLA contents.

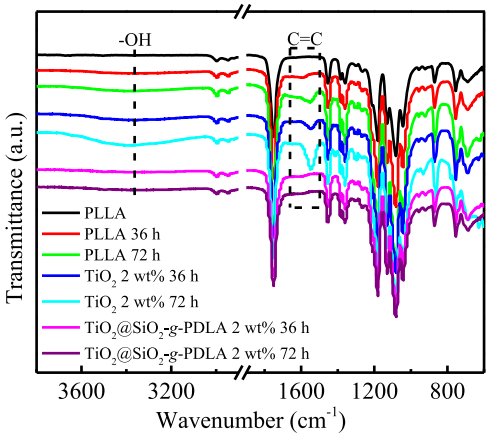

Figure 8. FTIR spectra of PLLA, PLLA/TiO_2, and PLLA/TiO_2@SiO_2-*g*-PDLA nanocomposites with different UV irradiation times.

Figure 2a shows the FT-IR spectra of TiO_2, TiO_2@SiO_2, and TiO_2@SiO_2-*g*-PDLA nanohybrids. The chemical structure of TiO_2@SiO_2 has been discussed above. Obviously, in the FT-IR spectrum of TiO_2@SiO_2-*g*-PDLA nanohybrids appear new peaks at 2800−3000 cm^{-1} owing to the symmetric and asymmetric stretching vibrations of the C−H bond and a peak at 1189 cm^{-1} corresponding to the stretching vibrations of the

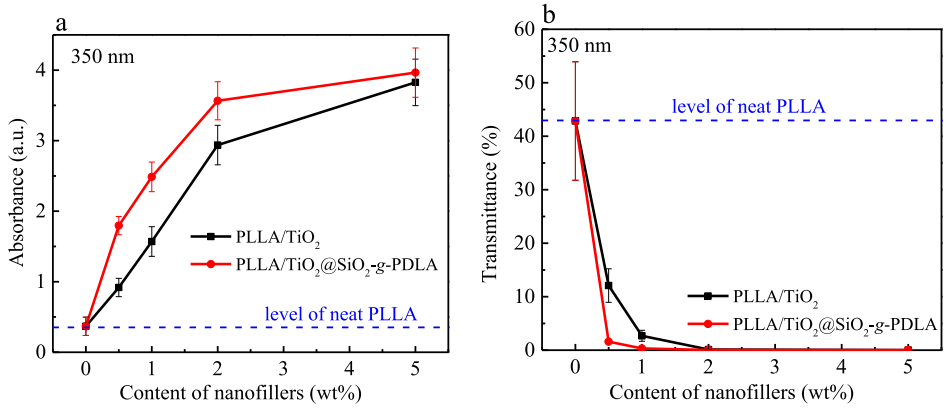

Figure 7. (a) UV absorption value and (b) transmittance at 350 nm as a function of nanofiller content in PLLA/TiO_2 and PLLA/TiO_2@SiO_2-*g*-PDLA nanocomposites.

https://dx.doi.org/10.1021/acsami.0c14423
ACS Appl. Mater. Interfaces 2020, 12, 49090−49100

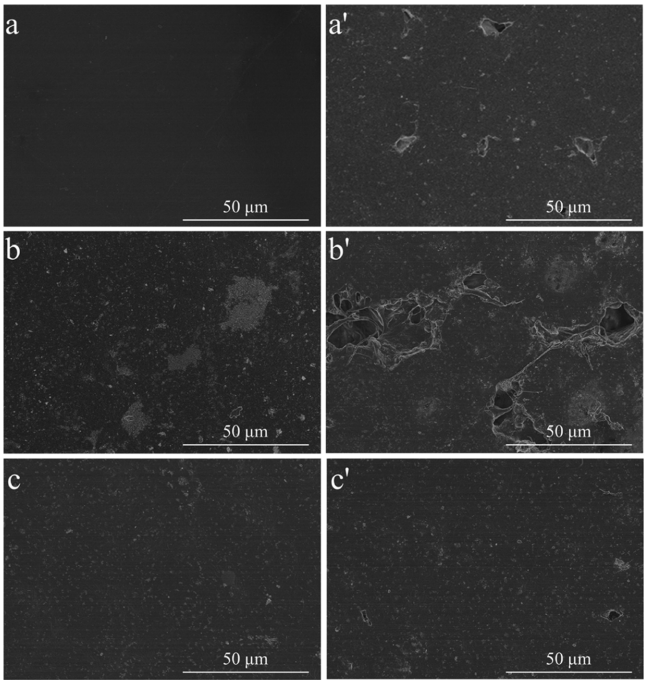

Figure 9. SEM images of the surface of (a/a') PLLA, (b/b') PLLA/TiO_2 (2 wt %), and (c/c') PLLA/TiO_2@SiO_2-*g*-PDLA nanocomposites before (a,b,c) and after UV irradiation (a',b',c').

C−O bond.[36] In addition, the new peak at 1750 cm^{-1} confirms the carbonyl stretching vibrations of PDLA chains on the surface of TiO_2@SiO_2-*g*-PDLA.[37] These new peaks indicate that PDLA was successfully grafted onto theTiO_2@SiO_2 nanoparticles. Moreover, the grafting reaction could be visually observed from the dispersion of nanohybrids in the solvent.[38] The images of a physical mixture of TiO_2@SiO_2 and PDLA (A) and of TiO_2@SiO_2-*g*-PDLA nanohybrids (B) in chloroform are shown in Figure 2b. Apparently, the bottom layer observed in bottle (A) is TiO_2@SiO_2 because of its insolubility and higher density, while TiO_2@SiO_2-*g*-PDLA nanohybrids could be effectively stabilized in chloroform by the grafted PDLA chains. Combined with FT-IR results, it verified the successful preparation of TiO_2@SiO_2-*g*-PDLA nanohybrids. This conclusion is also consistent with the XRD results, as shown in Figure 2c. Compared with TiO_2, TiO_2@SiO_2 has a weaker X-ray diffraction signal due to the surface coating of the SiO_2 layer. It has to be noted that TiO_2@SiO_2-*g*-PDLA nanohybrids show a new diffraction peak at 16.5°, which corresponds to the (200)/(110) crystal plane of grafted PDLA molecules.[39]

Furthermore, TGA measurements are used to characterize the coating and grafting degrees quantitatively, as shown in Figure 2d. TiO_2 does not show a significant weight loss below 1000 °C, while TiO_2@SiO_2 shows a weight loss corresponding to the SiO_2 layer until 700 °C. This is attributed to the loss of physically adsorbed water, reduction of O−H on the surface of TiO_2@SiO_2, and the decomposition of the residual organic groups (−CH_3CH_2) of the TEOS.[40] Convincingly, the TiO_2@SiO_2-*g*-PDLA nanohybrids show an obvious weight loss corresponding to the grafted PDLA in a temperature range of 260−400 °C. According to the differences in weight loss behavior,[41] the grafting degrees of the SiO_2 layer and PDLA chains are estimated as 5.3 and 20.5 wt %, respectively.

3.2. Morphology of the Double-Shell Structures of TiO_2@SiO_2-*g*-PDLA Nanohybrids. The morphology of TiO_2, TiO_2@SiO_2, and TiO_2@SiO_2-*g*-PDLA nanohybrids was at first studied by TEM, as shown in Figure 3. It can be inferred from Figure 3a that the TiO_2 nanoparticles show an irregular shape with a size between 50 and 100 nm and a clear boundary. Compared with TiO_2, the TiO_2@SiO_2 particles show an obvious core−shell morphology with an average shell thickness of 8 nm (Figure 3b). The TiO_2@SiO_2 nanoparticles in Figure 3 look larger than pristine TiO_2 because of two reasons. First, the size of TiO_2 nanoparticles actually were not uniform and the size distribution of TiO_2 nanoparticles was broad. Therefore, the image is also associated with the location to taken (Figure S1). Second, the larger nanoparticles of TiO_2@SiO_2 or TiO_2@SiO_2-*g*-PDLA nanoparticles (Figure 3b,c, orange square region) are actually stacks of the corresponding nanoparticles, and the size of a single-grafted nanoparticle is still around or below 100 nm (Figure 3, see the indication by white arrows). Interestingly, a double-shell structure is observed in the case of TiO_2@SiO_2-*g*-PDLA nanohybrids showing an outer layer with an irregular shape as well, as shown in Figure 3c. In addition, the TEM image was taken after evaporation of the chloroform (see the Experimental Section), and during evaporation, the TiO_2@SiO_2-*g*-PDLA nanohybrids would gradually agglomerate/precipitate.

In combination with the preparation method and the above chemical structural analysis (FT-IR and XPS results), the inner shell is identified as SiO_2, which is responsible for blocking the photocatalytic activity of TiO_2, while the outer shell is attributed to the deposited PDLA chains which are responsible for the better compatibilization with the PLLA matrix, to be discussed below. The irregular shape of the deposited PDLA layer also indicates random initiating sites and grafting reactions of the PDLA.

AFM was used to further study the morphology of TiO_2 and TiO_2@SiO_2-*g*-PDLA nanohybrids. As shown in Figure 4a, TiO_2 nanoparticles were distributed in a separate manner on a silicon wafer substrate, and the size of TiO_2 is between 50 and 100 nm with a clear boundary. This morphology is consistent with the TEM results (Figure 3a). The surface of TiO_2@SiO_2-*g*-PDLA nanohybrids in Figure 4b is rougher than that of TiO_2 due to the random distribution of PDLA chains on the surface, in line with the TEM images in Figure 3c.

Using the so-called modulus mode, different components can be easily distinguished by AFM, for example, the brighter phase in the images of Figure 4a'/b' indicates a relatively higher modulus component, and vice versa. It can be seen from Figure 4a'/b' that the TiO_2 nanoparticles with the clear boundary are much brighter, and thus, possess a higher modulus compared with the silicon substrate. However, the TiO_2@SiO_2-*g*-PDLA nanohybrids show a similar modulus with the silicon substrate because of the double-shelled structure, that is, SiO_2 and PDLA. Interestingly, all the TiO_2@SiO_2-*g*-PDLA nanohybrids are surrounded and interconnected by a low-modulus component (the dark phase in Figure 4b'), which is not observed in the peak force error mode (Figure 4b). It convincingly shows that the interpenetrated component with a low(er) modulus corresponds to the grafted PDLA phase considering the inherent moduli of TiO_2, SiO_2, and PDLA. Because of a dynamic reason, the grafted PDLA chains could not "stand" on the top or bottom of the nanoparticles after evaporation of the solvent, but the grafted PDLA chains were collapsed and absorbed to some extent on the substrate, as

https://dx.doi.org/10.1021/acsami.0c14423
ACS Appl. Mater. Interfaces 2020, 12, 49090−49100

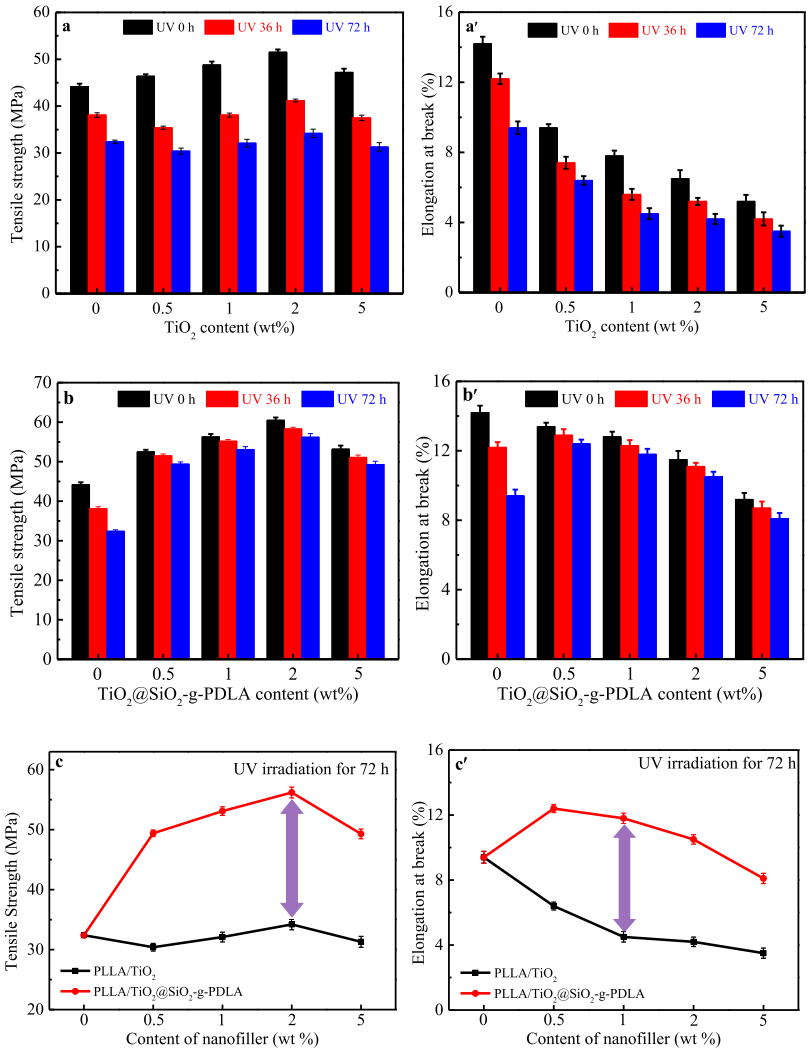

Figure 10. (a/b/c) Tensile strength and (a′/b′/c′) elongation at break of PLLA, PLLA/TiO_2, and PLLA/TiO_2@SiO_2-*g*-PDLA nanocomposites before and after UV irradiation.

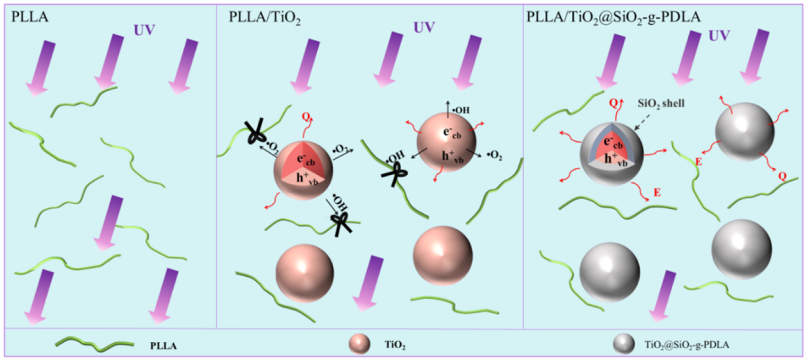

Figure 11. Schematic diagram of the UV resistance mechanism of PLLA nanocomposites, where *Q* and *E* represent the emitted heat and electromagnetic energy, respectively.

schematically illustrated in Figure 4c. Consequently, the TiO_2@SiO_2-*g*-PDLA nanohybrids exhibit a moderate modulus of the SiO_2 shell on the top (closer to the substrate), while a low(er) modulus of the PDLA shells was observed on the side. As also discussed in the Transmission Electron Microscopy section, the entanglement of PDLA chains makes the nanoparticles easier to be interconnected. These features ensure the interaction/entanglement of the grafted PDLA with the PLLA matrix in PLLA/TiO_2@SiO_2-*g*-PDLA nanocomposites.

3.3. Micromorphology of PLLA/TiO_2@SiO_2-*g*-PDLA Nanocomposites. The morphology of PLLA/TiO_2 and PLLA/TiO_2@SiO_2-*g*-PDLA nanocomposites was studied by TEM and AFM in the mode of peak force QNM properties, as shown in Figure 5.

https://dx.doi.org/10.1021/acsami.0c14423
ACS Appl. Mater. Interfaces 2020, 12, 49090−49100

As can be inferred from Figure 5a, the TiO_2 nanoparticles are aggregated, while the TiO_2@SiO_2-*g*-PDLA nanohybrids are uniformly dispersed in the PLLA matrix in Figure 5b, which is also confirmed by the AFM results in Figure 5a''/b''. In the peak force error images, the surface of the PLLA/TiO_2 nanocomposite (Figure 5a') is coarser in comparison with the PLLA/TiO_2@SiO_2-*g*-PDLA nanocomposite (Figure 5b'). Combined with the modulus images in Figure 5a''/b'', it can be distinguished that the bright phase represents TiO_2 and TiO_2@SiO_2-*g*-PDLA nanohybrids with a high(er) modulus, while the dark phase corresponds to the PLLA matrix with a low(er) modulus. The better dispersion of TiO_2@SiO_2-*g*-PDLA nanohybrids may result from the strong intermolecular interaction between the grafted PDLA chains and the PLLA matrix, that is, stereocomplexation. The stereocomplexation between the PLLA matrix and the TiO_2@SiO_2-*g*-PDLA nanohybrids can be confirmed by wide-angle XRD (WAXD) measurements, as shown in Figure 6. All X-ray patterns exhibit diffraction peaks at 2θ = 16.8 and 19°, which are assigned to the (200)/(110) and (203) planes of PLLA homocrystals (hc), respectively. The two diffraction peaks in the PLLA/TiO_2@SiO_2-*g*-PDLA nanocomposites are stronger compared with PLLA, indicating that the TiO_2@SiO_2-*g*-PDLA nanohybrids acting as nucleators could enhance the crystallization of PLLA. As expected, new diffraction peaks at 2θ = 12.2, 21, and 23.8° are observed for PLLA/TiO_2@SiO_2-*g*-PDLA nanocomposites, which correspond to the characteristic diffraction of (110), (300)/(030), and (220) planes of PLA stereocomplex crystallites (sc), respectively.[8] Moreover, measurements of PLLA nanocomposites were performed and are shown in Figure S2. During the heating process, a cold-crystallization peak (T_{cc}) and a melting peak ($T_{m\text{-}hc}$) at around 164 °C are observed for all the samples corresponding to the homocrystallites of PLLA. In the meantime, an additional melting peak at around 223 °C was detected only for the PLLA/TiO_2@SiO_2-*g*-PDLA nanocomposites, indicating the formation of sc. These WAXD and differential scanning calorimetry (DSC) results proved the stereocomplexation between the PLLA matrix and the TiO_2@SiO_2-*g*-PDLA nanohybrids, and the in situ-formed sc crystallites could further promote the crystallization of the PLLA matrix and the interfacial adhesion between the PLLA matrix and the TiO_2@SiO_2-*g*-PDLA nanoparticles and would enhance the mechanical properties of the PLLA nanocomposites.

It is also noticed from the AFM modulus images (Figure 5a''/b'') that the modulus of the TiO_2@SiO_2-*g*-PDLA nanohybrids is lower than that of the TiO_2 aggregates due to the grafted PDLA molecules. The lower modulus of the TiO_2@SiO_2-*g*-PDLA nanohybrids is ascribed to the "softer" PDLA shell outside of the nanohybrids and the finer embedment of the nanohybrids in the PLLA matrix. To summarize, the double-shelled TiO_2@SiO_2-*g*-PDLA nanohybrids have a finer and more homogeneous dispersion than those of TiO_2 nanoparticles in the PLLA nanocomposites because of the interfacial stereocomplexation.

3.4. UV Shielding and UV Resistance of PLLA/TiO_2@SiO_2-*g*-PDLA Nanocomposites. A UV−vis near-infrared spectrophotometer was used to study the UV-shielding behavior of the PLLA nanocomposites with different types of nanofillers. Figure 7a shows the UV absorption values of the PLLA nanocomposites at 350 nm as a function of the nanofiller content. It can be seen that the UV absorption values of both PLLA/TiO_2 and PLLA/TiO_2@SiO_2-*g*-PDLA nanocomposites increased monotonically with the increase of the nanofiller content. This is ascribed to the excellent UV absorbing property of TiO_2 nanoparticles. TiO_2 could absorb energy from UV light and then emitted as heat or electromagnetic radiation,[14] and thus, the UV-absorbing performance of the PLLA nanocomposites are enhanced with the TiO_2 content. In addition, the UV absorption values of the PLLA/TiO_2@SiO_2-*g*-PDLA nanocomposite are much higher than those of the PLLA/TiO_2 nanocomposite with the same nanofiller content. The better UV absorption performance of the PLLA/TiO_2@SiO_2-*g*-PDLA nanocomposite is also due to the fine and uniform dispersion of TiO_2@SiO_2-*g*-PDLA nanohybrids which generates larger specific surface areas. The UV transmittance of the material can be calculated according to the Lambert−Beer law $A = -\log T$[42] (where A and T represent the light absorbance and light transmittance, respectively) and the results are shown in Figure 7b. In general, the less the UV light transmittance of the material, the better its UV shielding performance. Obviously, 99.0% of the UV light for the PLLA/TiO_2@SiO_2-*g*-PDLA nanocomposite was shielded, whereas 96.7% of the UV light was shielded for PLLA/TiO_2 when the contents of nanofillers were both 1.0 wt %. Consequently, the PLLA/TiO_2@SiO_2-*g*-PDLA nanocomposite has a better UV-shielding property.

As discussed earlier, it is challenging to make UV-shielding PLA along with a UV-resistant performance which, however, is one of the main objectives of this work. Therefore, the UV resistance of the PLLA was evaluated by exposing it to UV irradiation. According to the literature, the decomposition reaction of PLA under UV light conforms to the Norrish II decomposition mechanism, that is, the breaking of the C−C bond and the formation of an alkene (or a ketone).[43−45] The chemical structures of PLLA, PLLA/TiO_2, and PLLA/TiO_2@SiO_2-*g*-PDLA nanocomposites were analyzed by FT-IR spectroscopy as a function of UV irradiation time (0, 36, and 72 h, respectively), as shown in Figure 8. It can be seen that PLLA, PLLA/TiO_2, and PLLA/TiO_2@SiO_2-*g*-PDLA nanocomposites all showed new infrared absorption peaks at 1590 and 3360 cm^{-1} after UV irradiation, which corresponded to the stretching vibration of the C=C bond and the O−H bond in carboxyl groups, respectively.[46] In addition, the intensity of FT-IR peaks corresponding to the C=C and O−H bonds of PLLA and PLLA/TiO_2 nanocomposites increased with UV irradiation time. Moreover, under the same UV irradiation time, the intensity of these two peaks of the PLLA/TiO_2 nanocomposite is stronger than that of the PLLA, indicating that TiO_2 accelerated the degradation of PLLA due to its photocatalytic activity. This phenomenon is consistent with the decomposition behavior of rhodamine B in Section 3.1. However, in the case of PLLA/TiO_2@SiO_2-*g*-PDLA nanocomposites, the two peaks are not so visible and the intensity did not change significantly with irradiation time, indicating an unobvious degradation of the PLLA matrix.

Moreover, SEM was used to detect the surface morphology of PLLA, PLLA/TiO_2, and PLLA/TiO_2@SiO_2-*g*-PDLA nanocomposites before and after UV irradiation for 72 h, as shown in Figure 9. The surface of PLLA is smooth before irradiation, and it becomes rough with cracks after 72 h of UV irradiation (Figure 9a/a'). Meanwhile, the surface of the PLLA/TiO_2 nanocomposite is much rougher with obvious cracks after the same amount of irradiation (Figure 9b') because the presence of TiO_2 promoted the degradation of the PLLA matrix. Compared with PLLA and PLLA/TiO_2 nanocomposites, the

https://dx.doi.org/10.1021/acsami.0c14423
ACS Appl. Mater. Interfaces 2020, 12, 49090−49100

surface of the PLLA/TiO_2@SiO_2-*g*-PDLA nanocomposite only changed slightly after UV irradiation for 72 h. Therefore, it can be concluded from the above FT-IR and SEM results that the PLLA/TiO_2@SiO_2-*g*-PDLA nanocomposite possesses excellent UV resistance in comparison with neat PLLA.

3.5. Mechanical Properties of PLLA Nanocomposites Affected by UV Irradiation. Figure 10 shows the mechanical properties of PLLA, PLLA/TiO_2, and PLLA/TiO_2@SiO_2-*g*-PDLA nanocomposites before and after UV irradiation for 36 and 72 h. It is shown that the tensile strength of PLLA/TiO_2 nanocomposites increased by 8 MPa when the content of TiO_2 increased from 0 to 2 wt % before UV irradiation, while an increase by 18 MPa was observed in the case of PLLA/TiO_2@SiO_2-*g*-PDLA nanocomposites (black pillars in Figure 10a/b). However, the tensile strength of PLLA nanocomposites decreased with the addition of 5 wt % TiO_2@SiO_2-*g*-PDLA nanoparticles. This is because TiO_2@SiO_2-*g*-PDLA could aggregate at a higher TiO_2@SiO_2-*g*-PDLA content (5 wt %), which may sacrifice its reinforcement efficiency. Obviously, the addition of nanoparticles reinforced the PLLA matrix, and the reinforcing effect of the TiO_2@SiO_2-*g*-PDLA nanohybrids is more significant because of the greatly improved compatibility via interfacial stereocomplexation. This advantage is also observed from the elongation at break of the nanocomposites (black pillars in Figure 10a'/b').

After UV irradiation for 72 h, the drop percentage in the tensile strength of PLLA, PLLA/TiO_2 (2 wt %), and PLLA/TiO_2@SiO_2-*g*-PDLA (2 wt %) nanocomposites was 27, 36, and 8%, respectively. Even after UV irradiation for 72 h, the PLLA/TiO_2@SiO_2-*g*-PDLA nanocomposite still showed higher tensile strength than neat PLLA before irradiation. The elongation at break of nanocomposites after UV irradiation for 72 h shows the same trend. Moreover, the PLLA/TiO_2-*g*-PDLA composites were prepared and the mechanical behavior as a function of UV irradiation time, that is, 0, 36, and 72 h, can be seen in Figure S3a. It shows that the tensile strength and elongation at break of PLLA/TiO_2-*g*-PDLA nanocomposites before UV irradiation were 57.3 MPa and 8.0, respectively, which decreased by 38 and 60% after UV irradiation for 72 h. As the grafted PDLA basically has the same physical and chemical characters as the PLLA matrix, the UV-resistant behavior of the PLLA/TiO_2-*g*-PDLA nanocomposite was comparable to that of the PLLA/TiO_2 nanocomposite (Figures 10 and S3b) although the grafted PDLA is beneficial to interfacial adhesion. Consequently, the UV resistance of PLLA/TiO_2@SiO_2-*g*-PDLA nanocomposites was investigated by using untreated TiO_2 as a reference. The differences in mechanical properties after UV irradiation for the PLLA and PLLA nanocomposites are due to the UV resistance of the PLLA nanocomposites with different types of TiO_2 nanoparticles, and it is well consistent with the FT-IR and SEM results in Figures 8 and 9. Therefore, the TiO_2@SiO_2-*g*-PDLA nanohybrids with double-shelled structures can significantly reinforce the PLLA matrix under both normal and UV irradiation conditions.

It has been proved that TiO_2 can induce the photocatalysis reaction in active oxygen species, that is, $^{\bullet}O_2$ and $^{\bullet}OH$ by oxidative or reductive reductions under UV conditions,[33,47,48] which has been proven by using the electron spin resonance technique in the literature.[47] These active oxygen species can further lead to a degradation reaction by attacking polyester chains such as PLA, and consequently, accelerate chain cleavage. This reaction mechanism has been proven in the polyester/TiO_2 system as well.[33,48] As shown in Figure 11, when the UV light is irradiated on the PLLA/TiO_2@SiO_2-*g*-PDLA nanocomposite, it cannot easily penetrate the whole nanocomposite because of the excellent UV-shielding property of the nanocomposite (Figure 7). It can be thought that the degradation of PLLA under UV irradiation only occurs on the surface. The difference is that in PLLA/TiO_2 nanocomposites, TiO_2 nanoparticles come in direct contact with the PLLA matrix, and the free radicals with high activity ($^{\bullet}O_2$ and $^{\bullet}OH$) generated by UV light will directly attack the PLLA, leading to the degradation of PLLA on the whole. However, in the PLLA/TiO_2@SiO_2-*g*-PDLA nanocomposites, the radicals are blocked by the inter-SiO_2 shell, which cannot directly attack the PLLA matrix. The energy of UV light absorbed by TiO_2@SiO_2-*g*-PDLA nanohybrids has eventually dissipated as the heat or electromagnetic energy. Therefore, the PLLA/TiO_2@SiO_2-*g*-PDLA nanocomposites exhibit not only excellent UV-shielding property but also superior UV resistance.

4. CONCLUSIONS

A novel strategy is demonstrated in this work to design PLLA/TiO_2@SiO_2-*g*-PDLA nanocomposites with improved mechanical strength, excellent UV-shielding property, and UV resistance. The double-shell structured TiO_2@SiO_2-*g*-PDLA nanohybrids, with an inner SiO_2 shell weight of 5.3 wt % and an outer PDLA shell of 20.5 wt %, were prepared by hydrolysis of TEOS and ring-opening polymerization of D-lactide, successively. The SiO_2 shell prevents nondesirable chemical reactions between the TiO_2 nanoparticles and the PLLA matrix, and the PDLA shell can easily interact with the PLLA matrix and facilitates the uniform dispersion of nanohybrids, thus leading to not only higher mechanical properties (increased the tensile strength by 49%) but also an enhancement in UV shielding and UV resistance of PLLA simultaneously. Therefore, this work provides a novel strategy to make advanced PLLA-based nanocomposites with potential in the application of durable packaging and special fiber/textile applications, and so forth.

■ ASSOCIATED CONTENT

Supporting Information

The Supporting Information is available free of charge at https://pubs.acs.org/doi/10.1021/acsami.0c14423.

TEM images of TiO_2 particles in different places; DSC first heating curves of PLLA and PLLA nanocomposites; and stress−strain curves of PLLA and PLLA nanocomposites under UV irradiation (PDF)

■ AUTHOR INFORMATION

Corresponding Author

Piming Ma − *The Key Laboratory of Synthetic and Biological Colloids, Ministry of Education, Jiangnan University, Wuxi 214122, China;* orcid.org/0000-0002-4597-0639; Email: p.ma@jiangnan.edu.cn

Authors

Ying Cao − *The Key Laboratory of Synthetic and Biological Colloids, Ministry of Education, Jiangnan University, Wuxi 214122, China*

Pengwu Xu − *The Key Laboratory of Synthetic and Biological Colloids, Ministry of Education, Jiangnan University, Wuxi 214122, China;* orcid.org/0000-0001-7094-1445

https://dx.doi.org/10.1021/acsami.0c14423
ACS Appl. Mater. Interfaces 2020, 12, 49090−49100

Pei Lv − *The Key Laboratory of Synthetic and Biological Colloids, Ministry of Education, Jiangnan University, Wuxi 214122, China*
Pieter Jan Lemstra − *The Key Laboratory of Synthetic and Biological Colloids, Ministry of Education, Jiangnan University, Wuxi 214122, China; PlemPolco B. V., HV Veldhoven 5502, The Netherlands*
Xiaoxia Cai − *The Key Laboratory of Synthetic and Biological Colloids, Ministry of Education, Jiangnan University, Wuxi 214122, China*
Weijun Yang − *The Key Laboratory of Synthetic and Biological Colloids, Ministry of Education, Jiangnan University, Wuxi 214122, China*
Weifu Dong − *The Key Laboratory of Synthetic and Biological Colloids, Ministry of Education, Jiangnan University, Wuxi 214122, China;* orcid.org/0000-0002-7432-8362
Mingqing Chen − *The Key Laboratory of Synthetic and Biological Colloids, Ministry of Education, Jiangnan University, Wuxi 214122, China*
Tianxi Liu − *The Key Laboratory of Synthetic and Biological Colloids, Ministry of Education, Jiangnan University, Wuxi 214122, China*
Mingliang Du − *The Key Laboratory of Synthetic and Biological Colloids, Ministry of Education, Jiangnan University, Wuxi 214122, China*

Complete contact information is available at: https://pubs.acs.org/10.1021/acsami.0c14423

Notes

The authors declare no competing financial interest.

■ ACKNOWLEDGMENTS

This work was supported by the National Natural Science Foundation of China (51873082, 52073123), Distinguished Young Natural Science Foundation of Jiangsu Province and the MOE & SAFEA 111 Project (B13025).

■ REFERENCES

(1) Gross, R. A.; Kalra, B. Biodegradable Polymers for the Environment. *Science* **2002**, *297*, 803−807.
(2) Nampoothiri, K. M.; Nair, N. R.; John, R. P. An Overview of the Recent Developments in Polylactide (PLA) Research. *Bioresour. Technol.* **2010**, *101*, 8493−8501.
(3) Zeng, Q.; Ma, P.; Su, X.; Lai, D.; Lai, X.; Zeng, X.; Li, H. Facile Fabrication of Superhydrophobic and Magnetic Poly (lactic acid) Non-Woven Fabric for Oil-Water Separation. *Ind. Eng. Chem. Res.* **2020**, *59*, 9127−9135.
(4) Chen, Y.; Yuan, D.; Xu, C. Dynamically Vulcanized Biobased Polylactide/Natural Rubber Blend Material with Continuous Cross-Linked Rubber Phase. *ACS Appl. Mater. Interfaces* **2014**, *6*, 3811−3816.
(5) Sun, X.-R.; Cao, Z.-Q.; Bao, R.-Y.; Liu, Z.; Xie, B.-H.; Yang, M.-B.; Yang, W. A Green and Facile Melt-Approach for Hierarchically Porous Polylactide Monoliths Based on Stereocomplex Crystallite Network. *ACS Sustainable Chem. Eng.* **2017**, *5*, 8334−8343.
(6) Wu, B.; Zeng, Q.; Niu, D.; Yang, W.; Dong, W.; Chen, M.; Ma, P. Design of Supertoughened and Heat-Resistant PLLA/Elastomer Blends by Controlling the Distribution of Stereocomplex Crystallites and the Morphology. *Macromolecules* **2019**, *52*, 1092−1103.
(7) Ma, P.; Lv, P.; Xu, P.; Du, M.; Zhu, H.; Dong, W.; Chen, M. Design of Bio-Based Conductive and Fast Crystallizing Nanocomposites with Controllable Distribution of Multiwalled Carbon Nanotubes via Interfacial Stereocomplexation. *Chem. Eng. J.* **2018**, *336*, 223−232.
(8) Xu, P.; Lv, P.; Wu, B.; Ma, P.; Dong, W.; Chen, M.; Du, M.; Ming, W. Smart Design of Rapid Crystallizing and Nonleaching Antibacterial Poly (Lactide) Nanocomposites by Sustainable Aminolysis Grafting and in Situ Interfacial Stereocomplexation. *ACS Sustainable Chem. Eng.* **2018**, *6*, 13367−13377.
(9) Liang, Y.-Y.; Xu, J.-Z.; Li, Y.; Zhong, G.-J.; Wang, R.; Li, Z.-M. Promoting Interfacial Transcrystallization in Polylactide/Ramie Fiber Composites by Utilizing Interfacial Stereocomplex Crystals. *ACS Sustainable Chem. Eng.* **2017**, *5*, 7128−7136.
(10) Fang, H.; Chen, X.; Wang, S.; Cheng, S.; Ding, Y. Enhanced Mechanical and Oxygen Barrier Performance in Biodegradable Polyurethanes by Incorporating Cellulose Nanocrystals with Interfacial Polylactide Stereocomplexation. *Cellulose* **2019**, *26*, 9751−9764.
(11) Huang, J.; Cao, L.; Yuan, D.; Chen, Y. Design of Novel Self-Healing Thermoplastic Vulcanizates Utilizing Thermal/Magnetic/Light-Triggered Shape Memory Effects. *ACS Appl. Mater. Interfaces* **2018**, *10*, 40996−41002.
(12) Torres, F.; Nazhat, S.; Sheikhmdfadzullah, S.; Maquet, V.; Boccaccini, A. Mechanical Properties and Bioactivity of Porous PLGA/TiO_2 Nanoparticle-Filled Composites for Tissue Engineering Scaffolds. *Compos. Sci. Technol.* **2007**, *67*, 1139−1147.
(13) Boccaccini, A. R.; Blaker, J. J.; Maquet, V.; Chung, W.; Jérôme, R.; Nazhat, S. N. Poly(D,L-lactide) (PDLLA) Foams with TiO_2 Nanoparticles and PDLLA/TiO_2-Bioglass® Foam Composites For Tissue Engineering Scaffolds. *J. Mater. Sci.* **2006**, *41*, 3999−4008.
(14) Carneiro, J. O.; Teixeira, V.; Nascimento, J. H. O.; Neves, J.; Tavares, P. B. Photocatalytic Activity and UV-Protection of TiO_2 Nanocoatings on Poly (Lactic Acid) Fibres Deposited by Pulsed Magnetron Sputtering. *J. Nanosci. Nanotechnol.* **2011**, *11*, 8979−8985.
(15) Guo, Q.; Ma, Z.; Zhou, C.; Ren, Z.; Yang, X. Single Molecule Photocatalysis on TiO_2 Surfaces. *Chem. Rev.* **2019**, *119*, 11020−11041.
(16) Al-Mamun, M. R.; Kader, S.; Islam, M. S.; Khan, M. Z. H. Photocatalytic Activity Improvement and Application of UV-TiO_2 Photocatalysis in Textile Wastewater Treatment: a Review. *J. Environ. Chem. Eng.* **2019**, *7*, 103248.
(17) Li, X.; Lv, J.; Li, D.; Wang, L. Rapid Fabrication of TiO_2@Carboxymethyl Cellulose Coatings Capable of Shielding UV, Antifog and Delaying Support Aging. *Carbohydr. Polym.* **2017**, *169*, 398−405.
(18) Hoffmann, M. R.; Martin, S. T.; Choi, W.; Bahnemann, D. W. Environmental Applications of Semiconductor Photocatalysis. *Chem. Rev.* **1995**, *95*, 69−96.
(19) Sheng, Y.; Yang, J.; Wang, F.; Liu, L.; Liu, H.; Yan, C.; Guo, Z. Sol-Gel Synthesized Hexagonal Boron Nitride/Titania Nanocomposites with Enhanced Photocatalytic Activity. *Appl. Surf. Sci.* **2019**, *465*, 154−163.
(20) Huang, J. Y.; Li, S. H.; Ge, M. Z.; Wang, L. N.; Xing, T. L.; Chen, G. Q.; Liu, X. F.; Al-Deyab, S. S.; Zhang, K. Q.; Chen, T.; Lai, Y. K. Robust Superhydrophobic TiO_2@Fabrics for UV Shielding, Self-Cleaning and Oil-Water Separation. *J. Mater. Chem. A* **2015**, *3*, 2825−2832.
(21) Dastjerdi, R.; Montazer, M.; Shahsavan, S. A Novel Technique for Producing Durable Multifunctional Textiles Using Nanocomposite Coating. *Colloids Surf., B* **2010**, *81*, 32−41.
(22) Chen, J. J.; Wang, Z. Y.; Qian, G. D.; Fan, X. P. Preparation and UV Shielding of Homogeneous Dispersion Nanometer TiO_2. *Mater. Prot.* **2003**, *36*, 7−9.
(23) Wang, T.; Isimjan, T. T.; Chen, J.; Rohani, S. Transparent Nanostructured Coatings with UV-Shielding and Superhydrophobicity Properties. *Nanotechnology* **2011**, *22*, 265708.
(24) Bocchini, S.; Fukushima, K.; Blasio, A. D.; Fina, A.; Frache, A.; Geobaldo, F. Polylactic Acid and Polylactic Acid-Based Nanocomposite Photooxidation. *Biomacromolecules* **2010**, *11*, 2919−2926.
(25) Kosowska, K.; Szatkowski, P. Influence of ZnO, SiO_2 and TiO_2 on the Aging Process of PLA Fibers Produced By Electrospinning Method. *J Therm. Anal. Calorim.* **2020**, *140*, 1769−1778.
(26) Tsuji, H.; Echizen, Y.; Nishimura, Y. Photodegradation of Biodegradable Polyesters: a Comprehensive Study on Poly(L-

Lactide) and Poly(ε-Caprolactone). *Polym. Degrad. Stab.* **2006**, *91*, 1128−1137.
(27) Nonato, R. C.; Mei, L. H. I.; Bonse, B. C.; Chinaglia, E. F.; Morales, A. R. Nanocomposites of PLA Containing ZnO Nanofibers Made by Solvent Cast 3D Printing: Production and Characterization. *Eur. Polym. J.* **2019**, *114*, 271−278.
(28) Zhang, T.; Yu, Q.; Wang, J.; Wu, T. Design and Fabrication of a Renewable and Highly Transparent Multilayer Coating on Poly-(Lactic Acid) Film Capable of UV-Shielding and Antifogging. *Ind. Eng. Chem. Res.* **2018**, *57*, 4577−4584.
(29) Huang, X.-J.; Zeng, X.-F.; Wang, J.-X.; Chen, J.-F. Transparent Dispersions of Monodispersed ZnO Nanoparticles with Ultrahigh Content and Stability for Polymer Nanocomposite Film with Excellent Optical Properties. *Ind. Eng. Chem. Res.* **2018**, *57*, 4253−4260.
(30) Zhuang, W.; Liu, J.; Hua Zhang, J.; Xing Hu, B.; Shen, J. Preparation, Characterization, and Properties of TiO_2/PLA Nanocomposites by In Situ Polymerization. *Polym. Compos.* **2009**, *30*, 1074−1080.
(31) Xie, W.; Pakdel, E.; Liu, D.; Sun, L.; Wang, X. Waste-Hair-Derived Natural Melanin/TiO_2 Hybrids as Highly Efficient and Stable UV-Shielding Fillers for Polyurethane Films. *ACS Sustainable Chem. Eng.* **2020**, *8*, 1343−1352.
(32) Fujiwara, K.; Kuwahara, Y.; Sumida, Y.; Yamashita, H. Fabrication of Photocatalytic Paper Using TiO_2 Nanoparticles Confined in Hollow Silica Capsules. *Langmuir* **2017**, *33*, 288−295.
(33) Nakayama, N.; Hayashi, T. Preparation and Characterization of Poly(L-Lactic Acid)/TiO_2 Nanoparticle Nanocomposite Films with High Transparency and Efficient Photodegradability. *Polym. Degrad. Stab.* **2007**, *92*, 1255−1264.
(34) Cheng, F.; Sajedin, S. M.; Kelly, S. M.; Lee, A. F.; Kornherr, A. UV-Stable Paper Coated with APTES-Modified P25 TiO_2 Nanoparticles. *Carbohydr. Polym.* **2014**, *114*, 246−252.
(35) Furusawa, T.; Honda, K.; Ukaji, E.; Sato, M.; Suzuki, N. The Microwave Effect on the Properties of Silica-Coated TiO_2 Fine Particles Prepared Using Sol-Gel Method. *Mater. Res. Bull.* **2008**, *43*, 946−957.
(36) Goffin, A.-L.; Raquez, J.-M.; Duquesne, E.; Siqueira, G.; Habibi, Y.; Dufresne, A.; Dubois, P. From Interfacial Ring-Opening Polymerization to Melt Processing of Cellulose Nanowhisker-Filled Polylactide-Based Nanocomposites. *Biomacromolecules* **2011**, *12*, 2456−2465.
(37) Wan, J.; Cai, W.; Feng, J.; Meng, X.; Liu, E. In Situ Decoration of Carbon Nanotubes with Nearly Monodisperse Magnetite Nanoparticles in Liquid Polyols. *J. Mater. Chem.* **2007**, *17*, 1188−1192.
(38) Molau, G. E. Heterogeneous Polymer Systems. I. Polymeric Oil-in-Oil Emulsions. *J. Polym. Sci., Part A: Gen. Pap.* **1965**, *3*, 1267−1278.
(39) Ma, P.; Jiang, L.; Xu, P.; Dong, W.; Chen, M.; Lemstra, P. J. Rapid Stereocomplexation between Enantiomeric Comb-Shaped Cellulose-g-Poly(L-lactide) Nanohybrids and Poly(D-lactide) From the Melt. *Biomacromolecules* **2015**, *16*, 3723−3729.
(40) Bai, Y.; Li, Z.; Cheng, B.; Zhang, M.; Su, K. Higher UV-Shielding Ability and Lower Photocatalytic Activity of TiO_2@SiO_2/APTES and its Excellent Performance in Enhancing the Photostability of Poly(P-Phenylene Sulfide). *RSC Adv.* **2017**, *7*, 21758−21767.
(41) Yu, Q.; Yang, W.; Wang, Q.; Dong, W.; Du, M.; Ma, P. Functionalization of Cellulose Nanocrystals with Gamma-MPS and its Effect on the Adhesive Behavior of Acrylic Pressure Sensitive Adhesives. *Carbohydr. Polym.* **2019**, *217*, 168−177.
(42) Haaland, D. M.; Easterling, R. G.; Vopicka, D. A. Multivariate Least-Squares Methods Applied to the Quantitative Spectral Analysis of Multicomponent Samples. *Appl. Spectrosc.* **1985**, *39*, 73−84.
(43) Shogren, R. L.; Doane, W. M.; Garlotta, D.; Lawton, J. W.; Willett, J. L. Biodegradation of Starch/Polylactic Acid/Poly (Hydroxyester-Ether) Composite Bars in Soil. *Polym. Degrad. Stab.* **2003**, *79*, 405−411.
(44) Ikada, E. Photo- and Bio-Degradable Polyesters. Photodegradation Behaviors of Aliphatic Polyesters. *J. Photopolym. Sci. Technol.* **1997**, *10*, 265−270.
(45) Carneiro, J. O.; Teixeira, V.; Nascimento, J. H. O.; Neves, J.; Tavares, P. B. Photocatalytic Activity and UV-Protection of TiO_2 Nanocoatings on Poly (Lactic Acid) Fibres Deposited by Pulsed Magnetron Sputtering. *J. Nanosci. Nanotechnol.* **2011**, *11*, 8979−8985.
(46) Van-Cong, D.; Trang, N. T. T.; Giang, N. V.; Lam, T. D.; Hoang, T. Effect of TiO_2-Crystal Forms on the Photo-Degradation of EVA/PLA Blend Under Accelerated Weather Testing. *J. Electron. Mater.* **2016**, *45*, 2536−2546.
(47) Kim, T. K.; Lee, M. N.; Lee, S. H. Development of Surface Coating Technology of TiO_2 Powder and Improvement of Photocatalytic Activity by Surface Modification. *Thin Solid Films* **2005**, *475*, 171−177.
(48) Man, C.; Zhang, C.; Liu, Y. Poly (Lactic Acid)/Titanium Dioxide Composites: Preparation and Performance Under Ultraviolet Irradiation. *Polym. Degrad. Stab.* **2012**, *97*, 856−862.

https://dx.doi.org/10.1021/acsami.0c14423
ACS Appl. Mater. Interfaces 2020, 12, 49090−49100